SLAC-PUB-4216
March 1987
(T/E)

Low Q^2 Radiative Bhabha Scattering at High Energies*

DEAN KARLEN

Stanford Linear Accelerator Center
Stanford University, Stanford, California 94305

Abstract

A study of the process, $e^+e^- \to e^+e^-\gamma$, where at least one electron scatters at a small angle is presented. Calculations of the process to order α^3 and α^4 are reviewed and compared with data from the PEP storage ring. An analysis of data from the Mark II detector shows good agreement with the order α^4 calculation for $e\gamma$ final states. Preliminary results from the ASP detector agree well with the order α^3 and α^4 predictions for single particle configurations.

Talk presented at the Lake Louise Winter Institute,
Lake Louise, Alberta, Canada, February 15-21, 1987

---

* Work supported by the Department of Energy, contract DE-AC03-76SF00515.

1. Introduction

Radiative Bhabha scattering, $e^+e^- \to e^+e^-\gamma$, is described in lowest order by the 8 diagrams shown in fig. 1. Low Q^2 radiative Bhabha scattering, which refers to small angle scattering of one of the electrons, is dominated by the t channel diagrams. The contribution from the Z^0 is small, so only QED diagrams need to be included, even at high energies.

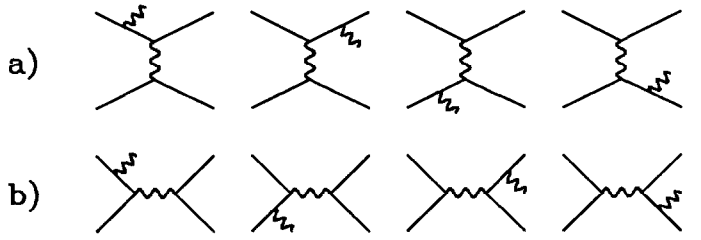

Figure 1. Order α^3 diagrams for radiative Bhabha scattering: a) t channel; b) s channel.

Since I consider small angle scattering of one of the electrons, there are three final state configurations, as shown in fig. 2. The $e\gamma$ configuration is useful as a luminosity measurement[1]; a deviation from the expected behavior could be a signal for composite electrons[2]. The single photon configuration is the primary background to neutrino counting experiments[3] which attempt to measure the single photon cross section from $e^+e^- \to \nu\bar{\nu}\gamma$. Both the single photon and single electron configurations are backgrounds to searches for supersymmetry[4].

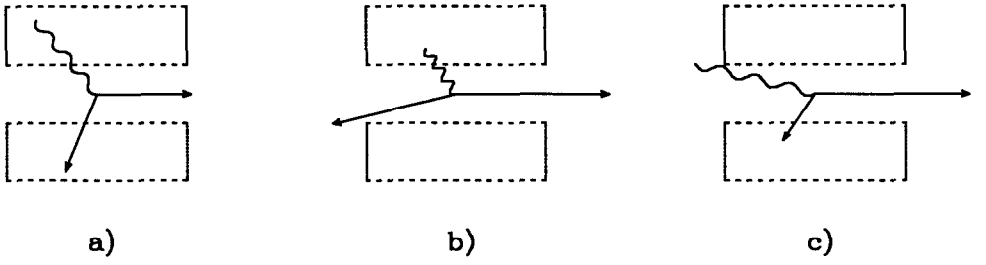

Figure 2. The three configurations for low Q^2 radiative Bhabha scattering, where the dashed boxes represent a detector: a) $e\gamma$; b) single γ; c) single e.

2. Order α^3 and α^4 Calculations

The calculation of the cross section from the eight diagrams of fig. 1 was first done by Swanson[5] in 1967 and later shown to have a compact form in the ultrarelativistic limit by Berends *et al.*[6,7]

Berends and Kleiss have written a Bhabha Monte Carlo event generator[7] which includes radiative Bhabha scattering as the next order correction. The program was not designed, however, to handle the configurations discussed above. The generation algorithm is inefficient for acollinear photon radiation and requires that the electrons scatter above a minimum angle. Also certain mass dependent terms that are important for low Q^2 are neglected in the cross section formula. Hence I found it necessary to write a Monte Carlo program[8] that includes the mass terms and has an event generation procedure that is efficient for low Q^2.

To describe more accurately radiative Bhabha scattering, one must consider the order α^4 correction. Both the virtual correction, shown in fig. 3a-d, and double radiative Bhabha scattering, shown in fig. 3e, need to be included in the calculation. This is a very complex problem, however, since there are more than 150 diagrams in this next order. The cross section for double radiative Bhabha scattering, described by 40 diagrams, has been evaluated[9], but a calculation of the virtual correction to radiative Bhabha scattering has not yet been published.

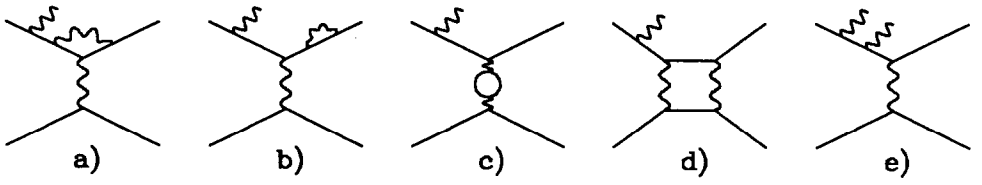

Figure 3. Some representative diagrams of the next order correction to radiative Bhabha scattering: a) Vertex correction; b) Electron self energy correction; c) Vacuum polarization; d) Box diagrams; e) Double radiative Bhabha scattering.

Since calculations for the exact treatment of radiative Bhabha scattering to order α^4 are not available, I make use of the equivalent photon approximation[10] along with the known radiative correction to Compton scattering. This method, valid only for low Q^2, includes just the diagrams shown in fig. 4, but this is

expected to be a good approximation of the total radiative correction[8]. This calculation is included in the Monte Carlo, and order α^3 and α^4 predictions from the program are presented in this talk.

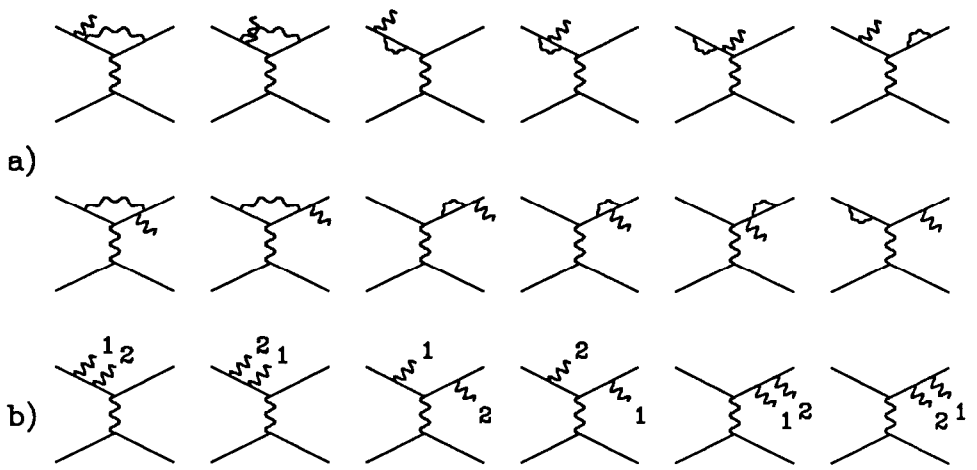

Figure 4. Diagrams included in the approximation of the radiative correction to radiative Bhabha scattering: a) Virtual correction diagrams; b) Double radiative Bhabha diagrams.

3. Comparison of the Monte Carlo With Data

3.1 $e\gamma$ CONFIGURATION

The Mark II detector[11] accumulated over 200 pb^{-1} of data at a center of mass energy of 29 GeV at the PEP storage ring[12]. The important elements of the detector used in the analysis of $e\gamma$ final states are the two concentric cylindrical drift chambers that provide a momentum resolution of $\delta p_\perp/p_\perp = \left[(.02)^2 + (.01p_\perp)^2\right]^{\frac{1}{2}}$ ($p_\perp$ in GeV/c) and the liquid argon electromagnetic calorimeter which has an energy resolution of $\delta E/E = .14/\sqrt{E}$ (E in GeV).

An electron and a photon are required to be inside the acceptance of the liquid argon calorimeter ($|\cos\theta| < .7$), have an acollinearity angle greater than 20 mrad and a coplanarity angle less than 80 mrad. The visible energy distribution of these events is shown in fig. 5 along with the order α^3 and α^4 Monte Carlo predictions. The minimum visible energy predicted by the order α^3 calculation is due to the kinematics of the three body final state since the two observed

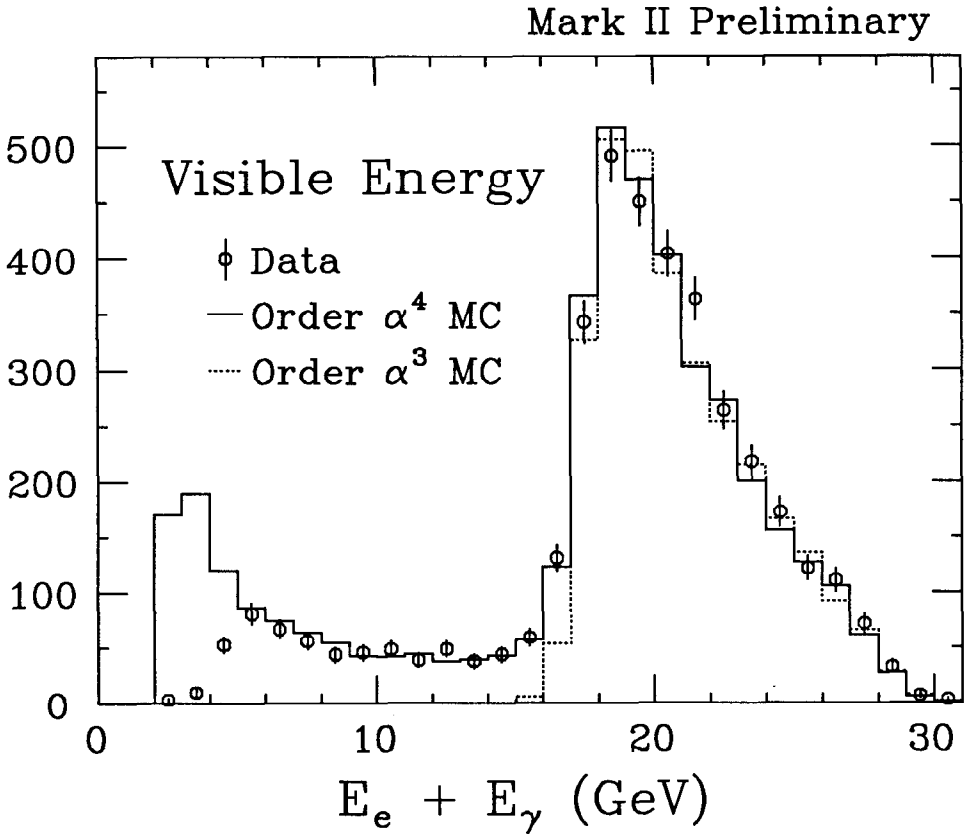

Figure 5. Visible energy for the $e\gamma$ configuration from the Mark II detector at PEP. The Monte Carlo curves represent the results after detector simulation and are normalized to the data. The discrepancy below 5 GeV is due to a first pass cut that is not included in the detector simulation.

particles must balance the longitudinal momentum of the small angle electron. The presence of a second photon releases this constraint in the order α^4 process.

Another distribution sensitive to the presence of a second photon is the χ^2 of the fit to a three body hypothesis. That is, using the precisely measured angles and assuming there are only three particles in the final state, it is possible to calculate the energies of the particles. The χ^2 of the measured energies for each event can then be calculated and the distribution is shown in fig. 6. This comparison to the Monte Carlo sample is sensitive to the detector simulation.

This preliminary analysis of Mark II data shows that the order α^4 calculation is necessary to describe accurately the $e\gamma$ configuration, and that the methods used to approximate this correction are valid.

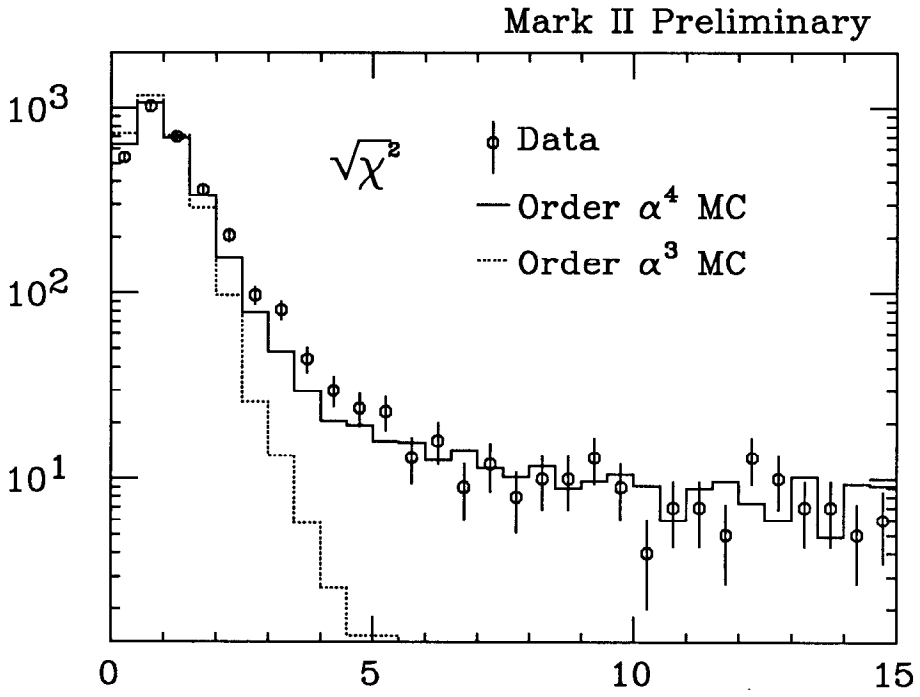

Figure 6. $\sqrt{\chi^2}$ for the constrained fit to a three body hypothesis. Again the Monte Carlo curves represent the results after detector simulation and are normalized to the data.

3.2 Single γ and Single e Configurations

A very preliminary analysis of the single e and single γ final states was carried out by the ASP collaboration[13] to check a surprising prediction* from the order α^4 calculation.

The ASP detector[14] was specially designed to detect anomalous single photon events at the PEP storage ring. The important elements used in the analysis of single particle configurations are the central tracker (five layers of proportional tubes, used to distinguish charged from neutral tracks), the central calorimeter (five layers of lead glass bars), and the forward drift chambers and calorimeters.

For this analysis, a single central track with $p_\perp > 1$ GeV/c is required to be inside the lead glass acceptance ($30° < \theta < 150°$) and no other tracks are

* The Monte Carlo program had predicted a very large contribution to the single γ cross section from fourth order. This has since been found to be due to an error in the event generation procedure. I thank M. Martinez and R. Miquel for assistance in finding the problem.

allowed to be above 150 mrad. In order to balance the central track $p_\perp$, at least one other particle must scatter above 35 mrad. Tracks between 21 and 150 mrad with $E > 4$ GeV are recorded as forward tracks. A data sample of 10 pb^{-1} is used in this analysis and the measured cross sections along with the order α^3 and α^4 Monte Carlo predictions are shown in table 1. Three topologies are considered; a charged or neutral central track with a single observed forward track, a neutral central track with a single observed forward track, and a charged or neutral central track with two observed forward tracks. In each case the data and Monte Carlo agree well. No attempt is made to include backgrounds from such sources as $e^+e^- \to \gamma\gamma\gamma$ and $e^+e^- \to e^+e^-e^+e^-$. Due to the preliminary nature of this analysis, systematic errors are not included.

Table 1. Comparison of single particle cross section measurements by ASP (preliminary) and predictions of the Monte Carlo. A central track has $p_\perp > 1$ GeV/c and is in the lead glass acceptance. A forward track has $E > 4$ GeV and is between 21 and 150 mrad from a beam axis.

	ASP	α^3	α^4
e or γ central, 1 forward	2.09 nb	2.10 nb	2.18 nb
γ central, 1 forward	0.19 nb	0.17 nb	0.17 nb
e or γ central, 2 forward	0.39 nb	0.40 nb	0.41 nb

Figures 7-9 show measured distributions of the single central–single forward track sample compared with the order α^3 and α^4 Monte Carlo predictions. In each case, the Monte Carlo results include the detector acceptance and simple energy smearing and are normalized to the measured integrated luminosity. Figure 7 shows the central track energy distribution as measured by the lead glass. The polar angle of the central track projected into the plane perpendicular to the lead glass array is shown in fig. 8 and in fig. 9 for the neutral central track only. This angle is measured with respect to the $+z$ or $-z$ axis according to the direction of the forward track. Figure 9 shows that the single photon is typically on the same side in z as the most scattered electron.

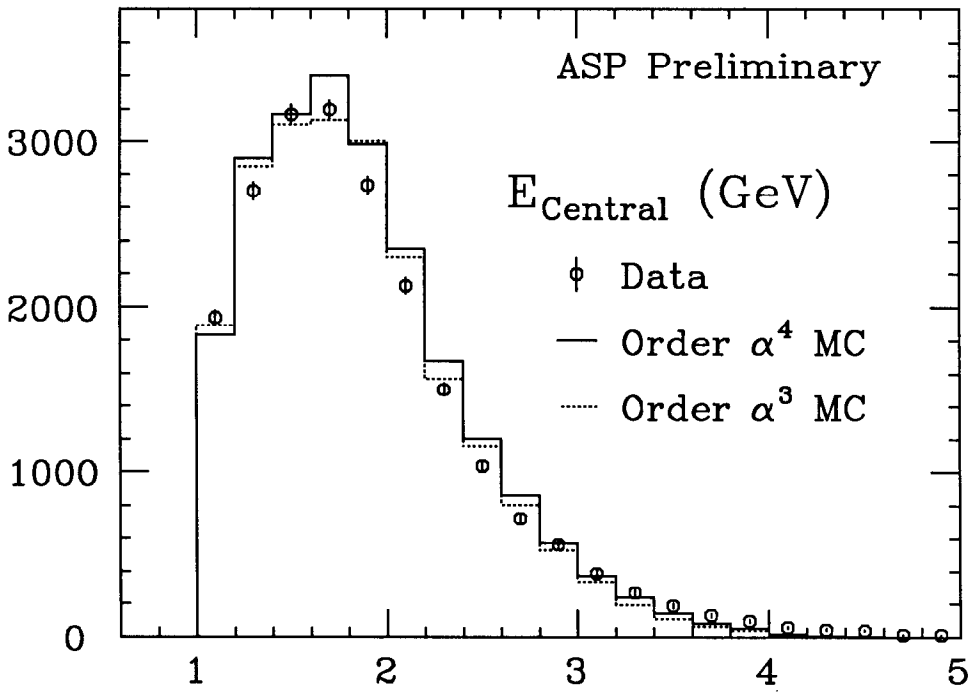

Figure 7. The neutral or charged central track energy distribution.

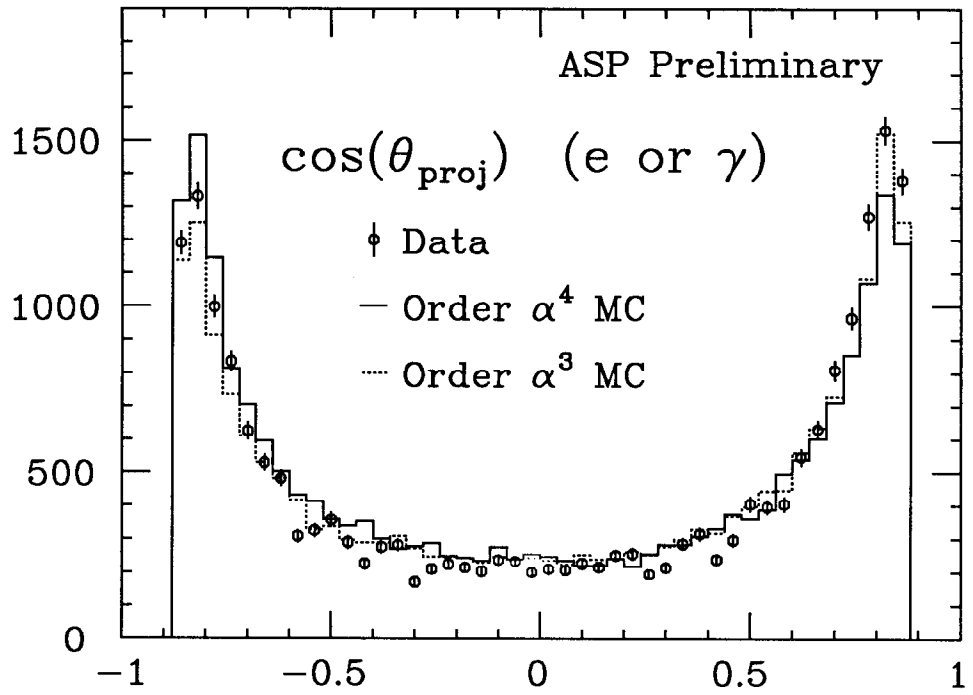

Figure 8. The cosine of the projected angle of the central neutral or charged track.

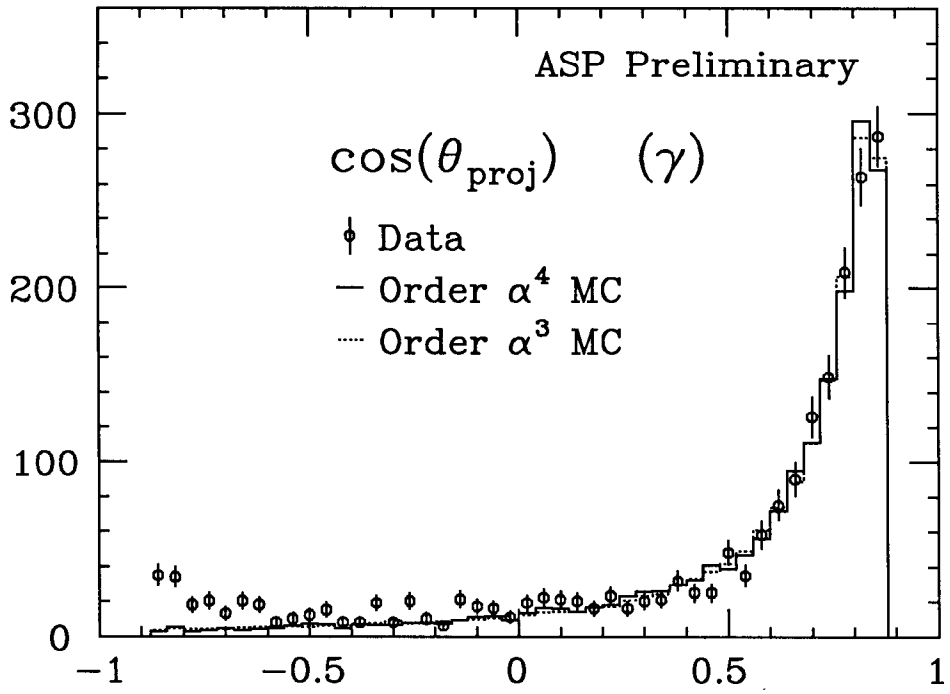

Figure 9. The cosine of the projected angle of the central neutral track.

4. Conclusions

I have reviewed calculations of low Q^2 radiative Bhabha scattering to order α^3 and α^4. In the case of the $e\gamma$ configuration, the order α^4 correction is well understood, so that it can provide another precise luminosity measurement at e^+e^- machines. For the single particle configurations, the contribution from order α^4 is seen to be small. The single photon background from radiative Bhabha scattering seems sufficiently understood so as not to limit the sensitivity of future neutrino counting experiments at SLC and LEP.

I would like to thank the ASP collaboration and especially T. Steele, for doing the analysis (with help from G. Bartha, D. Burke, C. Hawkins, and N. Roe) and for allowing me to present their preliminary results.

REFERENCES

1. A. Courau and P. Kessler, Phys. Rev. **D33** (1986) 2024.
2. H. Terazawa, M. Yasuè, K. Akama and M. Hayashi, Phys. Lett. **B112** (1982) 387;
   K. Hagiwara and D. Zeppenfeld, Z. Phys. **C29** (1985) 115.
3. E. Ma and J. Okada, Phys. Rev. Lett. **41** (1978) 287;
   K. Gaemers, R. Gastmans and F. Renard, Phys. Rev. **D19** (1979) 1605;
   G. Barbiellini, B. Richter and J. L. Siegrist, Phys. Lett. **B106** (1981) 414.
4. M. K. Gaillard, I. Hinchliffe and L. Hall, Phys. Lett. **B116** (1982) 279;
   P. Fayet, Phys. Lett. **B117** (1982) 460;
   J. Ellis and J. Hagelin, Phys. Lett. **B122** (1983) 303.
5. S. M. Swanson, Phys. Rev. **154** (1967) 1601.
6. F. A. Berends, R. Kleiss, P. De Causmaecker, R. Gastmans and T. T. Wu, Phys. Lett. **B103** (1981) 124.
7. F. A. Berends and R. Kleiss, Nucl. Phys. **B228** (1983) 537.
8. D. Karlen, SLAC preprint SLAC-PUB-4121 (1986).
9. F. A. Berends, P. De Causmaecker, R. Gastmans, R. Kleiss, W. Troost and T. T. Wu, Nucl. Phys. **B264** (1986) 265.
10. G. Bonneau and F. Martin, Nuovo Cim. **21A** (1974) 611;
    V. Gorgé, M. Locher and H. Rollnik, Nuovo Cim. **27** (1963) 928.
11. The Mark II detector is described in:
    R. H. Schindler, *et al.*, Phys. Rev. **D24** (1981) 78.
12. The members of the Mark II/PEP collaboration are:
    G. S. Abrams, D. Amidei, A. R. Baden, T. Barklow, A. M. Boyarski, J. Boyer, P. R. Burchat, D. L. Burke, F. Butler, J. M. Dorfan, G. J. Feldman, G. Gidal, L. Gladney, M. S. Gold, G. Goldhaber, L. J. Golding, J. Haggerty, G. Hanson, K. Hayes, D. Herrup, R. J. Hollebeek, W. R. Innes, J. A. Jaros, I. Juricic, J. A. Kadyk, D. Karlen, S. R. Klein, A. J. Lankford, R. R. Larsen, B. W. LeClaire, M. E. Levi, N. S. Lockyer, V. Lüth, C. Matteuzzi, M. E. Nelson, R. A. Ong, M. L. Perl, B. Richter, K. Riles, P. C. Rowson, T. Schaad, H. Schellman, W. B. Schmidke, P. D. Sheldon, G. H. Trilling, C. de la Vaissiere, D. R. Wood, and J. M. Yelton.
13. The members of the ASP collaboration are:
    G. Bartha, D. L. Burke, P. Extermann, P. Garbincius, C. A. Hawkins, C. Hearty, R. J. Hollebeek, A. S. Johnson, M. J. Jonker, L. Keller, C. Matteuzzi, N. A. Roe, J. E. Rothberg, T. R. Steele, J. S. Whitaker, R. J. Wilson, and K. K. Young.
14. The ASP detector is described in:
    G. Bartha, *et al.*, Phys. Rev. Lett. **56** (1986) 685.